Correlation of Polarizabilities with Van Der Waals Interactions in π-systems

Constantinos D. Zeinalipour-Yazdi* and David P. Pullman

San Diego State University, 5500 Campanile Drive, San Diego, California 92182-1030

Received: July 24, 2006; In Final Form: September 15, 2006

This work aims to (i) provide a semiquantitative relationship that can be used to estimate the binding energy, equilibrium separation, and potential energy surface (PES) for supermolecules consisting of benzene and small polycyclic aromatic hydrocarbons (PAHs) in parallel configuration and (ii) give a qualitative description of $\pi-\pi$ interactions between PAHs. We compute the one-dimensional PES of benzene translated parallel to various PAHs within the framework of second-order Møller−Plesset (MP2) perturbation theory. For PAHs of small MW difference, we observe a linear correlation between the binding energy and the number of carbon atoms in the supermolecule. The PES of these supermolecules is fit to an (exp-6) function whose variables are subsequently used to derive a mass-centered potential energy function as a function of the number of carbon atoms in the supermolecule. The linear dependence of the binding energy in the supermolecular series examined here can be directly correlated to the average polarizability product of the supermolecule. Last, we consider the supermolecular series of benzene with *n*-polyacenes to study the convergence of $\pi-\pi$ interactions between PAHs when their size is considerably different.

Introduction

Dispersion interactions are an important driving force for the supermolecular complexation and dynamics of PAHs in the condensed phase. These interactions govern the relative geometry and binding energy of the individual components in DNA,[1] proteins,[2] host−guest systems,[3] self-assembled supermolecular architectures,[4] in chemical and biological recognition,[5] and are responsible for aggregation phenomena.[6,7] Fundamental understanding and computational modeling of dispersion interactions in $\pi-\pi$ systems of unsubstituted PAHs, which lack other weak interactions such as dipole−dipole, dipole−induced dipole, and hydrogen-bonds, can be essential to other more complex chemical and biological systems where the dispersion interaction is only part of the overall interaction. Dispersion interactions are generally attributed to molecular polarization effects as expected from the classical London equation. A recent study by Sherill et al.,[8] on the interaction energy between substituted benzene molecules showed that both electron withdrawing and electron donating substituents result in a stronger attraction. This attraction was attributed to the effect of dispersion rather than electrostatic interactions. Additionally, polarization effects are well documented in the cation$-\pi$ interaction and have been used as a force for molecular recognition in aqueous media.[9]

X-ray diffraction studies of solid benzene,[10] naphthalene,[11,12] pyrene,[13] and coronene[14] and other planar PAHs[15] show the coexistence of two distinct relative configurations of the molecules. Molecules in these crystals appear in parallel-displaced and "T-shaped" configurations, and the attractive forces are attributed mainly to $\pi-\pi$ interactions and quadrupole−quadrupole[16] interactions, respectively. Both interactions seem to be equally important in small supermolecules of PAHs, but the former dominates in larger systems such as graphite.

Weak $\pi-\pi$ interactions are generally hard to measure experimentally because they are only a very small fraction of the total energy. Thus, any experiment that will probe these interactions must not excite intramolecular vibrations or induce structural changes whose energies will considerably exceed that of weak interactions. Only recent isothermal desorption spectroscopy of PAHs from the basal plane of graphite have proven successful in quantifying these interactions experimentally.[17] Furthermore, spectroscopic experiments in supersonic jet expansions have been able to provide significant information on the dominating equilibrium structures of the benzene dimer.[18−23] The benzene dimer has served as the model system for $\pi-\pi$ interactions because its relatively small size makes spectroscopic data easier to interpret and high-level computations feasible. In the literature, extensive experimental[18−23] and computational[24−35] studies exist that examine the conformation and binding energy of the benzene dimer. Hobza et al.[30] reports similar binding energies for the parallel-displaced and T-shaped configurations, and Tsuzuki et al.[35] showed the existence of a possible low-energy (∼0.2 kcal/mol) interconversion path between the configurations. The face-to-face configuration exhibits binding but is somewhat higher in energy[31] than the other conformations. Lee et al.[36] examined the supermolecular series of benzene, naphthalene, and anthracene dimers, where the authors find a linear relationship between the binding energy and the geometric overlap of the $\pi-\pi$ pairs. Here, we show that, for PAHs with small size difference, the binding energy depends linearly on the average molecular polarizability, and furthermore, the molecular polarizability is a linear function of the number of carbon atoms in each PAH. Finally, we derive a mass-centered potential energy function that can be used to obtain a semiquantitative PES for supermolecules consisting of benzene and small new PAHs.

First, we compute the basis set superposition error (BSSE) corrected PES of benzene and various PAHs at the MP2 level of theory. Then potential energy functions commonly employed in molecular mechanics (MM) force fields are fitted to the ab initio data. Subsequently, a simplified potential energy function is derived that describes the PES in these supermolecules as a

* Corresponding author. E-mail address: zeinalip@ucy.ac.cy. Current address: University of Cyprus, 75 Kallipoleos Street, P.O. Box 20537, 1678 Nicosia, Cyprus.

10.1021/jp064681h CCC: $33.50
Published on Web 11/07/2006

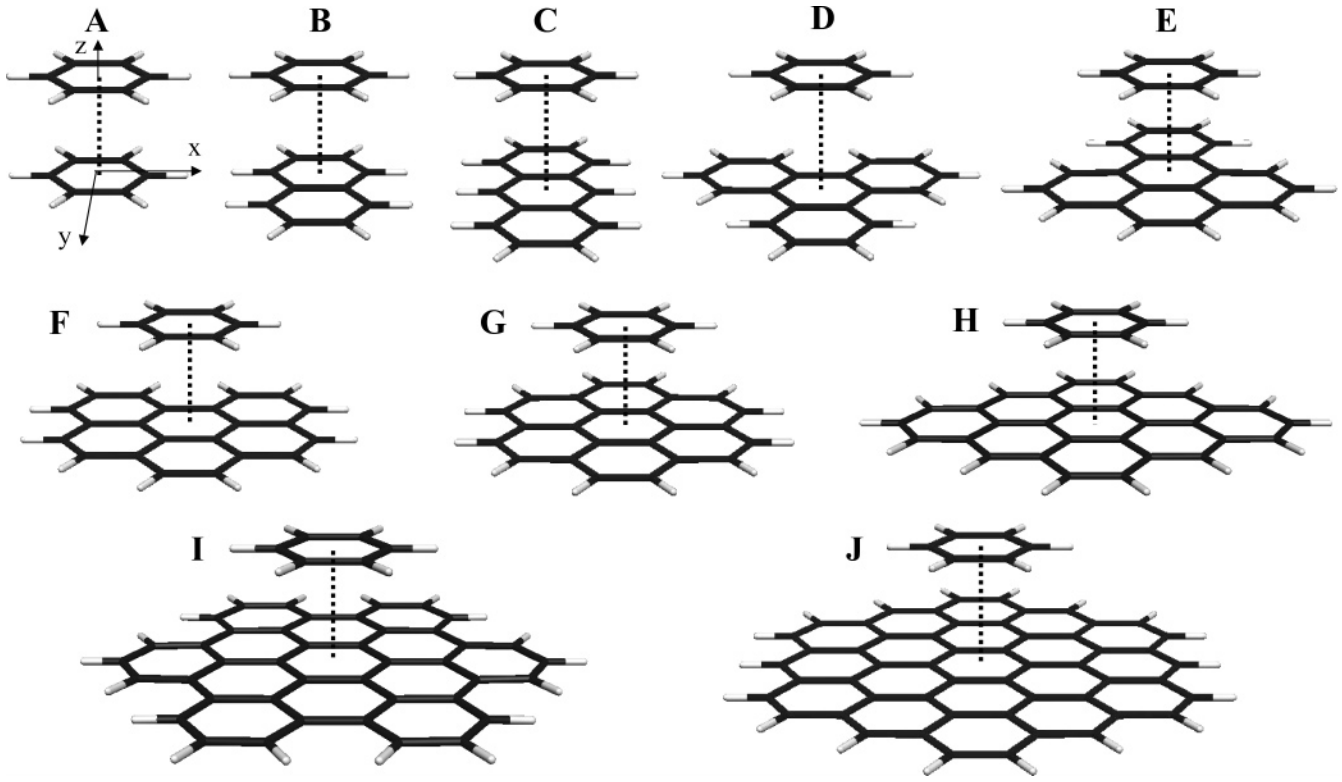

Figure 1. Schematic representation of PAH superstructures. Their nomenclature is provided in Table 1. The center of mass of benzene is centered above the underlying ring indicated by the dashed lines.

function of the number of carbon atoms in the supermolecule. This relationship could be broadly applied in the design of host−guest systems and supermolecular architectures where predictive equations that do not involve computationally demanding ab initio methods are desirable. A simplified equation of this type where the only input is the number of carbon atoms of the supermolecule is currently not available in the literature. We also compute the polarizability of the PAHs to examine (a) the correlation of the polarizability to the number of carbon atoms in the PAH and (b) the binding energy of benzene with a series of *n*-polyacenes as a function of the number of carbon atoms in the supermolecule to show at which point the interaction completely converges.

Computational Details

Basis set quality and level of correlation treatment are crucial for achieving quantitative agreement with experiment. Augmentation of the basis with diffuse functions and the addition of polarization functions have been proven necessary[37] to provide adequate variational flexibility to the one-electron wave functions. High-level correlated methods, such as CCSD(T), are also necessary to quantitatively describe the quantum mechanics of dispersion interactions.[31] While density functional methods are applicable to the large systems considered here, they typically underestimate the dispersion interactions between molecules and in most cases are completely repulsive.[38] Because our primary focus is to obtain *qualitative* trends in the binding energy with respect to molecular size in large supermolecules for which high-level correlated methods with large basis sets are prohibitive, we chose to carry out our calculations within the MP2 formalism.

All PAH geometries, except that of circumcoronene, were optimized at the MP2[39] level within the Cartesian correlation-consistent polarized valence double-ζ basis set (cc-pVDZ) by Dunning.[40] The structure of circumcoronene was optimized with the same basis, but by using density functional theory within the generalized gradient approximation using the PBE96[41] exchange-correlation functional. The 1s orbitals on carbons were frozen in all single-point energy and polarizability calculations as well as geometry optimizations. In the case of the benzene dimer, this had only a minimal effect on the computed binding energy. The root-mean-square of the energy gradient (GRMS) and energies were converged to 10^{-5} hartrees/bohr and 10^{-9} hartrees, respectively. The BSSE-corrected 1D PES scans were computed at the same level of theory by translating the rigid molecules along the supermolecular axis shown in Figure 1. To correct the BSSE, we employed the full counterpoise method by Boys and Bernardi.[42] All geometry optimizations and potential energy surface scans were carried out using NWChem[43] 4.6, and static polarizabilities were computed using the finite field method (FF) implemented in GAMESS.[44] The latter were carried out at electric field strengths of 0.000 au, $\pm$0.001 au and $\pm$0.002 au (0.001 au = 5.14×10^8 V/m). For all the molecules, the first hyperpolarizability (β_{uu}) was found to be about 4 orders of magnitude lower than the polarizability and is thus not reported.

Results and Discussion

The supermolecules investigated consist of a series of PAHs bound to benzene (Figure 1). All PAHs in this study are closed-shell molecules with planar molecular structures, and calculated C−C and C−H bond lengths range from 1.393 to 1.467 and 1.091−1.094 Å, respectively. Full BSSE-corrected PESs for selected PAH supermolecules are shown in Figure 2, and the corresponding binding energy (BE) and equilibrium separation using MP2/cc-pVDZ in Table 1. The energy was sampled at a higher resolution around the equilibrium region to accurately map out the PES. Non-BSSE-corrected PESs showed similar qualitative features, although deeper physisorption wells and shorter equilibrium separations were observed. Upon BSSE

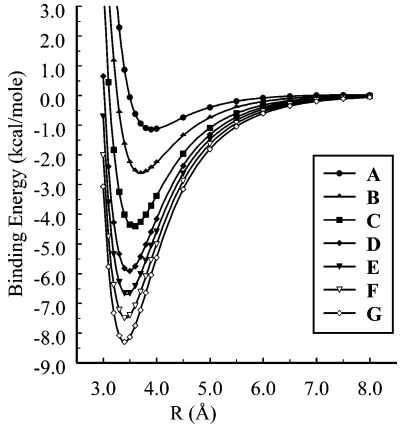

Figure 2. BSSE-corrected PES of benzene with various PAHs. Molecular structures and nomenclature are given in Figure 1 and Table 1, respectively. Single-point energy calculations are carried out in increments of 0.5 and 0.1 Å for 4.0 Å < R < 8.0 Å and 3.0 Å < R < 4.0 Å, respectively, where R is the separation between benzene and the supermolecule.

TABLE 1: BSSE-Corrected Binding Energy (D_e) and Equilibrium Separation (r_e) of Benzene and Various PAHs (A−J) at MP2/cc-pVDZ Level of Theory[a]

	supermolecule	D_e (kcal/mol)	r_e (Å)
A	benzene−benzene	−1.13	3.92
B	naphthalene−benzene	−2.61	3.70
C	anthracene−benzene	−4.40	3.56
D	triphenylene−benzene	−5.91	3.48
E	3,5-dihydro-benzo[*e*]pyrene−benzene	−6.69	3.45
F	1,3,5,10-tetrahydro-benzo[*ghi*]perylene−benzene	−7.49	3.42
G	coronene−benzene	−8.28	3.40
H	$C_{30}H_{20}$−benzene	−9.18	3.39
I	$C_{48}H_{18}$−benzene	−10.27	3.38
J	circumcoronene−benzene	−11.00	3.38

[a] For supermolecules H−J, only a few energy points around the estimated equilibrium (3.39 Å) separation were computed.

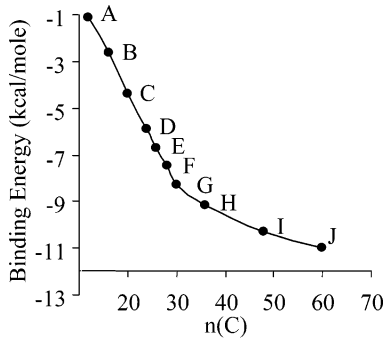

Figure 3. Binding energy as a function of the number of carbon atoms for supermolecules A−J.

correction, the physisorption well depth decreased by approximately 40%, and the equilibrium separation increased by a few tenths of an angstrom. The $\pi-\pi$ interactions become noticeably more pronounced for higher molecular weight supermolecules, and the binding energy increases by almost an order of magnitude upon increasing the supermolecule from benzene to circumcoronene. It is interesting to note that the binding energy of the circumcoronene−benzene system (11.00 kcal/mol) is only 5% smaller than the experimental activation energy[17] barrier for desorption of benzene from graphite (11.52 kcal/mol). For supermolecules A−G (Figure 3) we observe a near-linear correlation between BE and the equilibrium separation and the number of carbon atoms in the supermolecule. Nonetheless, for supermolecules H−J, the BE starts to converge. We therefore use the data for the supermolecules A−G to derive a semiquantitative relationship for their PES. Furthermore, we will show that an increasingly large size difference is necessary to obtain a complete convergence of the interaction.

i. Potential Energy Function Fit. Analytical potential energy functions with fitted parameters have been widely used as the dispersion interaction term in molecular mechanics force fields as they significantly decrease the computational expense and time in various simulations. Thus, we examined which empirical form for the potential energy function shows better agreement with our calculated ab initio data. The functions considered were various (m,6)-Lennard-Jones ((m,6)-LJ) potentials[45]

$$V(r) = \epsilon\cdot\left(\left(\frac{r_o}{r}\right)^m - \left(\frac{r_o}{r}\right)^6\right) \qquad m = 8, 9, 10, 11, \text{and } 12 \tag{1}$$

with fitting parameters ϵ and r_o and the (exp-6) function used by Fritz London[46] in the case of helium dimer

$$V(r) = \mathrm{A}\cdot e^{-\mathbf{B}\cdot r} - \frac{\mathrm{C}}{r^6} \tag{2}$$

with fitting parameters A, B, and C. The tolerance for the partial derivative, objective function, and fitting parameters were set to 5×10^{-5}, 1×10^{-9}, and 1×10^{-5}, respectively. The fitting parameter A was found to be invariant ($4.8\cdot10^5$ kcal/mol) with respect to the supermolecular size. Thus, only B and C are displayed in Tables 2 and 3. On the basis of R-squared values and visual inspection of the fitted curves, the (exp-6) potential energy function provided the best agreement with our ab initio data. The exponential repulsive term in this potential energy function seems to better capture the exponentially decaying nature of wave functions. For large separations, a minimal deviation of the fitted curve is observed. Although the functions in eqs 1 and 2 approach zero from below as r approaches infinity, the ab initio data displayed a negligible potential energy barrier of roughly 0.02 kcal/mol before converging to 0.00 kcal/mol at a separation of 16 Å.

The (12,6)-LJ potential function is sometimes preferred over the general (m,6)-LJ due to the more efficient evaluation of the potential (once $(r_o/r)^6$ is evaluated, the square power of that yields the repulsive contribution to the total energy). Compared to the (exp-6) potential, the absence of the exponential term significantly reduces the computational time associated with function evaluations in LJ-type potentials. However, because the LJ-type function resulted in a poor fit, we suggest that its use in molecular mechanics force fields should be judged with care when strong dispersion interactions, such as $\pi-\pi$ interactions, are involved. Nevertheless, if the use of a Lennard-Jones potential is necessary, then from the various (m,6)-LJ potentials examined here, the (9,6)-LJ (Table 3) gave the best fitting to the MP2 data.

Upon plotting the fitting parameters B and C as a function of the number of carbon atoms in the supermolecular complex, a linear relationship is observed (Figures 4 and 5). We make use of this linear relationship to derive a potential energy function that estimates the binding energy and equilibrium separation between small-molecular-weight PAHs as well as provide semiquantitative potential energy curves

$$V_{\mathrm{disp}}(\mathrm{C,sp^2}) = 4.8\cdot10^5\cdot e^{(0.008\cdot n(\mathrm{C})-3.41)\cdot r} - \frac{(1.12\cdot n(\mathrm{C}) - 4.6)\cdot10^3}{r^6} \tag{3}$$

TABLE 2: Fitting Parameters and *R*-Squared Values for (exp-6) Potential Energy Function

	supermolecule	B (1/Å)	C (10^3·kcal·Å^6/mol)	*R*-squared
A	benzene−benzene	3.32 ± 0.05	8.1 ± 0.3	0.9996
B	naphthalene−benzene	3.27 ± 0.04	13.3 ± 0.3	0.9994
C	anthracene−benzene	3.23 ± 0.03	18.8 ± 0.3	0.9994
D	triphenylene−benzene	3.21 ± 0.03	22.3 ± 0.3	0.9995
E	3,5-dihydro-benzo[*e*]pyrene−benzene	3.20 ± 0.02	24.3 ± 0.3	0.9997
F	1,3,5,10-tetrahydro-benzo[*ghi*]perylene−benzene	3.18 ± 0.02	26.3 ± 0.2	0.9998
G	coronene−benzene	3.16 ± 0.01	28.6 ± l 0.2	0.9999

TABLE 3: Lennard-Jones (9,6)-Potential Well Depth (ϵ) and Separation at $V = 0$ of Supermolecules

	supermolecule	ϵ (kcal/mol)	r_o (Å)	*R*-squared
A	benzene−benzene	7.8 ± 0.2	3.508 ± 0.007	0.999
B	naphthalene−benzene	17.0 ± 0.3	3.258 ± 0.003	0.998
C	anthracene−benzene	28.9 ± 0.3	3.111 ± 0.002	0.997
D	triphenylene−benzene	39.3 ± 0.3	3.020 ± 0.002	0.997
E	3,5-dihydro-benzo[*e*]pyrene−benzene	44.9 ± 0.3	2.988 ± 0.002	0.998
F	1,3,5,10-tetrahydro-benzo[*ghi*]perylene−benzene	50.6 ± 0.3	2.961 ± 0.002	0.998
G	coronene−benzene	56.3 ± 0.3	2.943 ± 0.003	0.998

where the $V_{disp}(C,sp^2)$ has units of kcal/mol, the distance r is in Å, and n(C) is the number of carbon atoms in the supermolecule. It must be noted that this equation is expected to work better for small PAH supermolecules because the linear relationship becomes a converging one in supermolecules of great size difference. We will elaborate on this behavior in a subsequent section.

ii. Static Polarizability Computations. Static polarizability calculations reveal the extent of electron density polarization that can occur when an electric field is applied in a certain direction. Table 4 summarizes the calculated static polarizabilities for benzene through coronene along the three Cartesian axes centered at the molecular center of mass (see Figure 1).

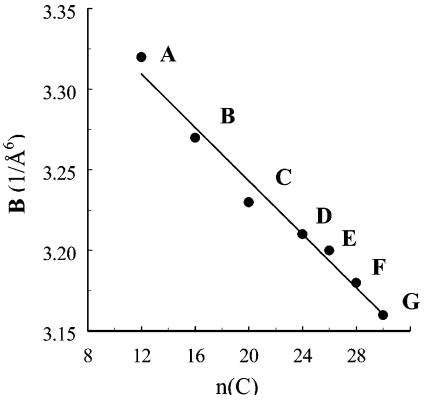

Figure 4. Fitting parameter B as a function of the number of carbon atoms in the supermolecule. The slope and intercept are (−0.0083 ± 0.0005) 1/Å^6 and (3.41 ± 0.01) 1/Å^6, respectively.

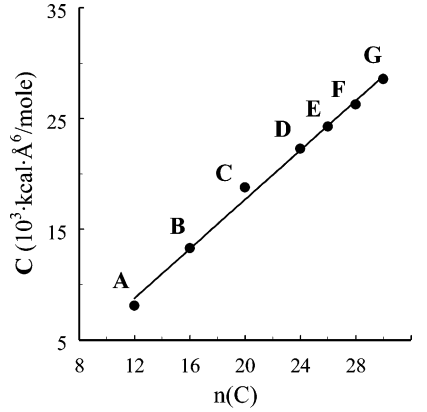

Figure 5. Fitting parameter C as a function of the number of carbon atoms in the supermolecule. The slope and intercept are (1.12 ± 0.04)·10^3·kcal·Å^6/mol and (4.6 ± 0.9)·10^3·kcal·Å^6/mol, respectively.

The average static polarizability of benzene (9.53×10^{-40} C^2·m^2/J) was 20% lower than the average polarizability of liquid benzene calculated using refractive index data[47] and the Clausius−Mossotti relation[48] (11.67×10^{-40} C^2·m^2/J), and it is in slightly better agreement with more reliable Kerr effect polarizability measurements (11.01×10^{-40} C^2·m^2/J). Deviations from Kerr effect[49] measurements were mostly in the computed perpendicular component (α_{zz}) of the polarizability tensor for benzene. Considering the modest size of our chosen basis and the fact that polarizabilities in the liquid phase are averaged over various solvation spheres, these deviations from experimental results are reasonable. The in-plane polarizability components (α_{xx} and α_{yy}) have the most significant contribution to the average polarizability, which indicates the greater ease of distorting the π-clouds in the *xy* plane. An additional feature of the computed polarizabilities is their linear scaling with the number of carbon atoms in the supermolecule as well as the binding energy (Figure 6). As expected from the classical London equation, the linear scaling between polarizabilities and n(C) explains also the linear correlation between binding energy and n(C) seen in the previous section.

iii. Convergence of Interaction. We observe that, for the first series of supermolecules, the linear trend of the binding energy with respect to the molecular size starts to converge after coronene. This convergence is expected because the linear relationship would imply infinite binding of benzene on graphite. Since complete convergence of the interaction would be computationally demanding, we tested higher symmetry and relatively lower molecular weight supermolecules to understand the extent to which $\pi-\pi$ interactions perturb the underlying PAH. This was carried out on the homologous supermolecular series of face-to-face benzene on (n)-polyacene where $n = 1$, 3, 5, 7, 9 and 11 (Figure 7).

In the hendecacene−benzene system, the binding energy is only marginally greater (a few tenths of a kcal/mol) than in the nonacene−benzene system. Figure 8 indicates that the binding energy reaches a limiting value as the size of the system becomes large.

We estimate the limiting values as 6.02 kcal/mol. On the basis of the potential energy curves shown in Figure 2, it is apparent

TABLE 4: Static Polarizability Components and Polarizability, $(\alpha_{xx} + \alpha_{yy} + \alpha_{zz})/3$, of Supermolecules Using MP2/cc-pVDZ[a]

PAH[b]	α_{xx} (au)	α_{yy} (au)	α_{zz} (au)	α_{PAH} (10^{-40} C^2·m^2/J)	α_{PAH}-α_{Bz}[c] (10^{-78} C^4·m^4/J^2)	C atoms[d]
benzene	74.05	74.05	25.23	9.53	0.91	12
naphthalene	113.29	156.20	38.88	16.95	1.62	16
anthracene	150.98	270.42	52.43	26.04	2.48	20
triphenylene	260.95	260.95	65.11	32.26	3.07	24
3.5-dihydro-benzo[*e*]pyrene	293.09	298.99	75.42	36.69	3.50	26
1.3.5.10-tetrahydro-benzo[*ghi*]perylene	344.46	320.47	75.85	40.71	3.88	28
coronene	372.74	372.74	81.28	45.44	4.33	30

[a] Only core electrons on heavy atoms are frozen. [b] Cartesian coordinate axis given in Figure 1. [c] Average polarizability of benzene (α_{Bz}). [d] Number of C atoms in supermolecule.

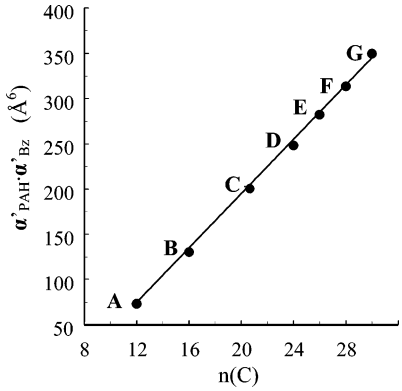

Figure 6. Polarizability volume product as a function of the number of carbon atoms in the supermolecule.

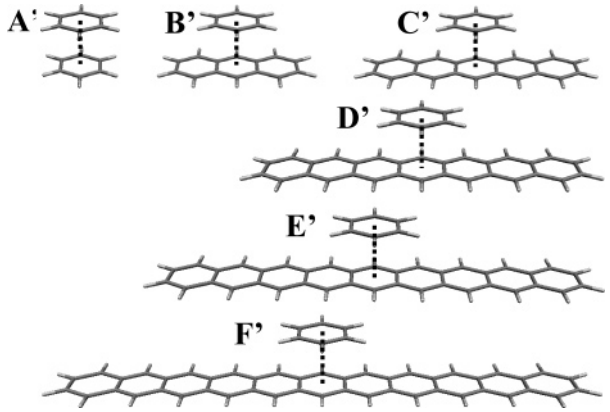

Figure 7. Schematic representation of benzene with *n*-polyacene superstructures, where *n* is 1, 3, 5, 7, 9, and 11. Benzene center of mass centered with respect to underlying ring.

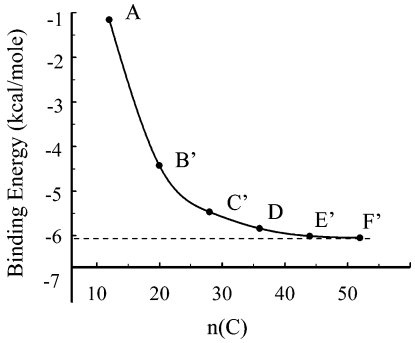

Figure 8. BSSE-corrected dispersion interactions for *n*-polyacene−benzene supermolecular series.

that, at an intermolecular distance larger than 8 Å, additional stabilization of a supermolecule through dispersion interactions will not be observed. However, stabilization still occurs in the supermolecular systems when *n* is increased from 9 to 11. In other words, perturbations to the electron distribution of hendecacene's edge rings happen even at 13.5 Å separations from the benzene molecule. To show that these perturbations occur through the delocalized π−cloud and not through the direct interaction of the benzene molecule and the edge rings, we performed the following computation. We obtained the PES of three benzene molecules that had the following configuration. One maintained the same position as benzene in the supermolecule. The other two were placed in the position of the edge rings in hendecacene. We observe a minimum in the PES at 4.0 Å that is less than a thousandth of a kcal/mol. This suggests that the increase in binding energy going from $n = 9$ to $n = 11$ is a result of perturbations of the edge MOs in hendecacene caused from adjacent MOs that are in closer proximity to benzene and not from the direct interaction of benzene with the edge rings. The perturbations of the edge rings from adjacent MOs at separations as large as 13.5 Å can be attributed to the delocalized nature of the π-system. For this reason, separations larger than this are suggestive for the pairwise interactions evaluation cutoff parameter in MM simulations.

Conclusions

MP2 potential energy surface scans for benzene and two series of polycyclic aromatic hydrocarbons (PAHs) are obtained. The binding energy at equilibrium separation shows a linear relationship with the number of carbon atoms in the supermolecules A−G. We provide an explanation for the linear scaling of the binding energy with the size of the supermolecule by studying the molecular polarizabilities of the PAHs (A−G) under investigation. The static polarizabilities show a similar linear dependence with the number of carbon atoms in the supermolecule.

Various potential energy functions commonly employed in molecular mechanics force fields are fitted to the MP2 data, and the (exp-6) function yields the best agreement. The LJ potentials, except the (9,6) potential, exhibit poor fitting and should be used with care when trying to describe the effects of $\pi-\pi$ interactions. We use the (exp-6) potential to derive a simplified relationship that only depends on the number of carbon atoms and yet is capable of providing relatively accurate PESs for small-molecular-weight PAHs supermolecules.

Computations on the homologous supermolecular series of face-to-face benzene on (*n*)-polyacene where $n = 1, 3, 5, 7, 9$ and 11 revealed that large separations are required to observe convergence of $\pi-\pi$ interactions. This may be attributed to the ease with which electron density can be shifted in the delocalized π-system of PAHs. We suggest the use of a cutoff radius of at least 13.5 Å in MM summations.

The linear relationship becomes a converging one when the relative size difference of the PAHs in the supermolecule becomes large (H−J and C′−F′), which can be attributed to the increased separation of benzene and the edge of the

supermolecule. This affects the extent to which benzene can polarize the larger PAH. Future work involves the derivation of atom pairwise fitting parameters A and B that will be calibrated for MM type calculations.

Acknowledgment. We thank Dr. Greg Gidofalvi for useful discussions and PURE Bioscience of El Cajon, CA for partial funding support of the computer resources.

Supporting Information Available: Cartesian coordinates of the supermolecules used in this work. This material is available free of charge via the Internet at http://pubs.acs.org.

References and Notes

(1) Sponer, J.; Hobza, P. *Chem. Phys. Lett.* **1997**, *267*, 263.
(2) Burley, S. K.; Petsko, G. A. A*dv. Prot. Chem.* **1988**, *39*, 125.
(3) Smithrud, D. B.; Diederich, F. *J. Am. Chem. Soc.* **1990**, *112*, 339.
(4) Fyfe, M. C. T.; Stoddart, J. F. *J. Phys. Org. Chem.* **1997**, *10*, 254.
(5) Meyer, E. A.; Castellano, R. K.; Diederich, F. *Angew. Chem., Int. Ed.* **2003**, *42*, 1210.
(6) Alexander, A. E. *J. Chem. Soc.* **1937**, 1813.
(7) Hughes, A. *Proc. R. Soc. London, Ser. A* **1936**, *155*, 710.
(8) Ringer, A. L.; Sinnokrot, M. O.; Lively, R. P.; Sherrill, D. C. *Chem.—Eur. J.* **2006**, *12*, 3821.
(9) Gallivan, J. P.; Dougherty, D. A. *Proc. Natl. Acad. Sci. U.S.A.* **1999**, *96*, 9459.
(10) Bacon, B. E.; Curry, N. A.; Wilson, S. A. *Proc. R. Soc. London, Ser. A* **1964**, *279*, 98.
(11) Abrahams, S. C.; Robertson, J. M.; White, J. G. *Acta Crystallogr.* **1949**, *2*, 233.
(12) Frampton, C. S.; Knight, K. S.; Shankland, N.; Shankland, K. *J. Mol. Struct.* **2000**, *520*, 29.
(13) Robertson, J. M.; White, J. G. *J. Chem. Soc.* **1947**, *72*, 358.
(14) Robertson, J. M.; White, J. G. *J. Chem. Soc.* **1945**, *164*, 607.
(15) Desiraju, G. R.; Gavezzotti, A. *Acta Crystallogr., Sect. B* **1989**, *45*, 473.
(16) Hunter, C. A., Sanders J. K. M. *J. Am. Chem. Soc.* **1990**, *112*, 5525.
(17) Zacharia, R.; Ulbricht, H.; Hertel, T, *Phys. Rev. B* **2004**, *69*, 155406.
(18) Law, K. S.; Schauer, M.; Bernstein, E. R. *J. Chem. Phys.* **1984**, *81*, 4871.
(19) Krause, H.; Ernstberger, B.; Neusser, H. J. *Chem. Phys. Lett.* **1991**, *184*, 411.
(20) Aruan, E.; Gutowsky, H. S. *J. Chem. Phys.* **1992**, *98*, 4294.
(21) Venturo, V. V.; Felker, P. M. *J. Chem. Phys.* **1993**, *99*, 748.
(22) Špirko, V.; Engkvist, O.; Soldán, P.; Selzle, H. L.; Schlag, E. W.; Hobza, P. *J. Chem. Phys.* **1999**, *111*, 572.
(23) Kenneth, C. J.; Hemminger, J. C.; Winn, J. S.; Novick, S. E.; Harris, S. J.; Klemperer, W. *J. Chem. Phys.* **1975**, *63*, 1419.
(24) Pawliszyn, J.; Szezesniak, M. M.; Scheiner, S. *J. Phys. Chem.* **1984**, *88*, 1726.
(25) Hobza, P.; Selzle, H. L.; Schlag, E. W. *J. Chem. Phys.* **1990**, *93*, 5893.
(26) Hobza, P.; Selzle, H. L.; Schlag, E. W. *J. Chem. Phys.* **1993**, *97*, 3937.
(27) Hobza, P.; Selzle, H. L.; Schlag, E. W. *J. Am. Chem. Soc.* **1994**, *116*, 3500.
(28) Hobza, P.; Selzle, H. L.; Schlag, E. W. *Chem. Rev.* **1994**, *94*, 1767.
(29) Jaffe, R. L.; Smith, G. D. *J. Chem. Phys.* **1996**, *105*, 2780.
(30) Hobza, P.; Selzle, H. L.; Schlag, E. W. *J. Phys. Chem.* **1996**, *100*, 18790.
(31) Tsuzuki, S.; Uchimaru, T.; Mastumura, K.; Mikami, M.; Tanabe, K. *Chem. Phys. Lett.* **2000**, *319*, 547.
(32) Gonzalez, C.; Lim, E. C. *J. Phys. Chem. A* **2000**, *104*, 2953.
(33) Tsuzuki, S.; Honda, K.; Uchimaru, T.; Mikami, M.; Tanabe, K. *J. Am. Chem. Soc.* **2002**, *124*, 104.
(34) Sinnokrot, M. O.; Valeev, E. F.; Sherill, C. D. *J. Am. Chem. Soc.* **2002**, *124*, 10887.
(35) Tsuzuki, S.; Uchimaru, T.; Sugawara, K.; Mikami, M. *J. Chem. Phys.* **2002**, *117*, 11216.
(36) Lee, K. L.; Park, S.; Kim, S. K. *J. Chem. Phys.* **2002**, *116*, 7910.
(37) Tsuzuki, S.; Uchimaru, T.; Tanabe, K. *J. Mol. Struct.* **1993**, *307*, 107.
(38) Tsuzuki, S.; Lüthi, H. P. *J. Chem. Phys.* **2001**, *114*, 3949.
(39) Møller, C.; Plesset, M. S. *Phys. Rev.* **1934**, *46*, 618.
(40) Dunning, T. H., Jr. *J. Chem. Phys.* **1989**, *90*, 1007.
(41) Perdew, J. P.; Burke, K.; Ernzerhof, M. *Phys. Rev. Lett.* **1997**, *78*, 1396.
(42) Boys, S. F.; Bernardi, F. *Mol. Phys.* **1970**, *19*, 553.
(43) Kendall, R. A.; Aprà, E.; Bernholdt, D. E.; Bylaska, E. J.; Dupuis, M.; Fann, G. I.; Harrison, R. J.; Ju, J.; Nichols, J. A.; Nieplocha, J.; Straatsma, T. P.; Windus, T. L.; Wong, A. T. *Comput. Phys. Commun.* **2000**, *128*, 260.
(44) Schmidt, M. W.; Baldridge, K. K.; Boatz, J. A.; Elbert, S. T.; Gordon, M. S.; Jensen, J. J.; Koseki, S.; Matsunaga, N.; Nguyen, K. A.; Su, S.; Windus, T. L.; Dupuis, M.; Montgomery, J. A. *J. Comput. Chem.* **1993**, *14*, 1347.
(45) Jones, J. E. *Proc. R. Soc. London, Ser. A* **1924**, *106*, 463.
(46) London, F. *Proc. R. Soc. London, Ser. A* **1936**, *153*, 576.
(47) $n = 1.524$ at 434 nm, $n = 1.501$ at 589 nm, $n = 1.497$ at 656 nm. Measurements taken from Gray, D. E. *American Institute of Physics Handbook*; McGraw-Hill: New York, 1972.
(48) Clausius−Mossotti relation $(\epsilon_r - 1)/(\epsilon_r + 2) = (\rho \cdot N_A \cdot \alpha)/(3 \cdot \epsilon_0 \cdot M)$ and $\epsilon_r = n^2$, where α is average polarizability, n average refractive index, ϵ_r relative permittivity, ρ density, N_A Avogadro's number, M molecular weight of medium, and ϵ_0 vacuum permittivity.
(49) Gentle, I. R.; Ritchie, L. D. *J. Chem. Phys.* **1989**, *93*, 7740.